

# Transient Thermal Analysis of 3-D Integrated Circuits Packages by the DGTD Method

Ping Li, *Senior Member, IEEE*, Yilin Dong, *Student Member, IEEE*, Min Tang, *Member, IEEE*, Junfa Mao, *Fellow, IEEE*, Li Jun Jiang, *Senior Member, IEEE*, and Hakan Bağcı, *Senior Member, IEEE*

**Abstract**—Since accurate thermal analysis plays a critical role in the thermal design and management of the 3-D system-level integration, in this paper, a discontinuous Galerkin time-domain (DGTD) algorithm is proposed to achieve this purpose. Such as the parabolic partial differential equation (PDE), the transient thermal equation cannot be directly solved by the DGTD method. To address this issue, the heat flux, as an auxiliary variable, is introduced to reduce the Laplace operator to a divergence operator. The resulting PDE is hyperbolic, which can be further written into a conservative form. By properly choosing the definition of the numerical flux used for the information exchange between neighboring elements, the hyperbolic thermal PDE can be solved by the DGTD together with the auxiliary differential equation. The proposed algorithm is a kind of element-level domain decomposition method, which is suitable to deal with multiscale geometries in 3-D integrated systems. To verify the accuracy and robustness of the developed DGTD algorithm, several representative examples are benchmarked.

**Index Terms**—Auxiliary-differential equation (ADE) method, discontinuous Galerkin time-domain (DGTD) method, integrated circuit package, numerical flux, transient thermal analysis.

## I. INTRODUCTION

**F**OLLOWING the Moore's law, the number of transistors in a single chip has raised from a few thousands in 1970s to several billions in 2010s, while the electrical size has been continuously downscaling. Further fueled by the advanced 3-D packaging technologies such as system on package [1], [2] and interconnection technologies like the through silicon-vias (TSV) [3], heterogeneous modules and chips are

capable of being vertically stacked up together by TSVs and redistribution traces, which thus makes the possibility to integrate multiple different functional modules into a limited space. On the other hand, it simultaneously brings significant challenges in the thermal management. Improper thermal designs would not only degrade the system performance, but also lead to serious reliability issues. Therefore, accurate and robust thermal analysis is essential at the design stage.

To achieve this purpose, numerous modalities have been proposed in the past decades to characterize the thermal properties of the integrated circuits, for instance, the analytical approaches [4] and numerical algorithms such as the finite element method (FEM) [5], [6] and finite difference method (FDM) [7]–[9]. The analytical method in [4] proposed an equivalent thermal circuit model to describe the temperature variation, which is convenient and efficient to provide a guideline at the design stage although it is not comprehensive and exactly rigorous. Recently, researchers proposed a noniterative heat transfer model [10], [11] to predict the steady-state temperature distributions in 3-D chips, the accuracy of the analytical method is comparable to FEM. On the other hand, the numerical methods are rigorous but less efficient. In [5] and [6], to handle the multiscale properties of the 3-D integrated circuit packages, a domain decomposition method (DDM)-based FEM was proposed, which converges significantly fast while conventional FEM would fail to converge. In [12]–[14], the efficiency of the FEM is further improved by the parallel computing techniques. Thus, more complicated structures can be modeled within less computational cost. Besides the FEM, in [7] and [8], the FDM was employed to facilitate the thermal analysis. Specifically, an equivalent circuit network was derived based on the FDM formulated equations in [9] that builds up the relation between thermal models and equivalent circuit networks. In [15] and [16], an FDM-based thermal solver named “HotSpot,” which is based on the equivalent circuit of thermal resistance and capacitances of microarchitecture blocks, is widely applied to analyze thermal distributions of integration circuits. Compared to the FEM, the FDM is more convenient and simple to implement, but lacks the flexibility to address irregular geometries.

In this paper, a discontinuous Galerkin time-domain (DGTD) method [17]–[20] is proposed to conduct the transient thermal analysis for complicated integrated circuits packages. Compared to the finite-difference time-domain method, the

Manuscript received May 31, 2016; revised November 10, 2016; accepted January 16, 2017. Date of publication March 10, 2017; date of current version May 31, 2017. This work was supported in part by the National Science Foundation of China under Grant 61234001 and Grant 61674105 and in part by the University Grants Council of Hong Kong under Contract AoE/P-04/08. Recommended for publication by Associate Editor A. Jain upon evaluation of reviewers' comments. (Ping Li and Yilin Dong contributed equally to this work.)

P. Li was with the Department of Electrical and Computer Engineering, Purdue University, West Lafayette, IN 47906 USA. He is now with the Department of Electrical and Electronic Engineering, The University of Hong Kong, Hong Kong (e-mail: liping@eee.hku.hk).

Y. Dong, M. Tang, and J. Mao are with the Department of Electronic Engineering, Shanghai Jiao Tong University, Shanghai 200240, China (e-mail: flystar-dyl@sjtu.edu.cn; tm222@sjtu.edu.cn; jfmao@sjtu.edu.cn).

L. J. Jiang is with the Department of Electrical and Electronic Engineering, The University of Hong Kong, Hong Kong (e-mail:jianglj@hku.hk).

H. Bağcı is with the Department of Electronic Engineering, King Abdullah University of Science and Technology, Thuwal 23955, Saudi Arabia (e-mail: hakan.bagci@kaust.edu.sa).

Color versions of one or more of the figures in this paper are available online at <http://ieeexplore.ieee.org>.

Digital Object Identifier 10.1109/TCPMT.2017.2666259

DGTD method is capable of modeling arbitrary shapes and simultaneously can achieve high-order accuracy by adopting hierarchical basis functions. Similar to the finite volume method [21], all operators in the DGTD analysis are local, and the information exchange between the neighboring mesh elements is implemented by a term called numerical flux. Therefore, unlike FEM, the matrix equations are locally established with dimension equal to the number of degrees of freedom in the corresponding mesh element. Thus, the formulated mass-matrices are block-diagonal and can be directly inverted with negligible computational cost. Since the solutions across the interfaces of adjacent elements are allowed to be discontinuous, the DGTD method owns more flexibilities to choose the type and the order of basis functions in each element [22]. In fact, the DGTD method can be considered as an element-level DDM. Therefore, the DGTD method is more preferable for large and/or multiscale geometries in which a large number of heterogeneous meshes are involved [23]. If the conventional FEM was used, the ill-conditioned matrix equations resulted from inhomogeneous mesh elements would converge very slowly or even not converge at all. Alternatively, the complicated domain decomposition FEM has to be resorted [5], [6].

Since the DGTD method is amenable to the hyperbolic systems, the thermal equation as a parabolic partial differential equation (PDE) is thus unable to be solved by the DGTD algorithm directly [17]. To handle this problem, an auxiliary variable named heat flux is introduced with the aim to degenerate the high-order spatial differential operator (Laplace operator  $\nabla^2$ ) to a first-order operator (divergence operator  $\nabla \cdot$ ). Then, the thermal equation is transformed to be a hyperbolic PDE that can be written into a conservative form. Together with the differential equation governing the auxiliary variable, the newly constructed thermal equation can be solved by the DGTD method. To validate the feasibility, the accuracy, and the robustness of the developed DGTD method, several representative examples including the 3-D integration with complex structures are given.

The remainder of this paper is organized as follows. In Section II, the theory and mathematical details about the degeneration of the parabolic equation to a hyperbolic one and the formulation matrix equations by the DGTD method are described. In Section III, numerical examples are presented to validate the proposed algorithm. Conclusions and discussions are given at the end of this paper.

## II. THEORY AND MATHEMATICAL FORMULATION

Suppose that the domain of interest for the thermal analysis is denoted as  $\Omega$  and simultaneously bounded by the boundary  $\partial\Omega$ , its temporal temperature variation in this thermal system is governed by a first-order time-derivative PDE defined as [5], [12]

$$\nabla \cdot \kappa \nabla T + Q = \rho_m c_\rho \frac{\partial T}{\partial t} \quad (1)$$

where  $T$  denotes the temperature distribution,  $\kappa$  represents the thermal conductivity,  $Q$  is the heat source, and  $\rho_m$  and  $c_\rho$  are the mass density of the material and specific heat

capacity, respectively. To solve (1), we have the Dirichlet boundary condition at the boundary  $\partial\Omega$

$$T = T_{\delta\Omega} \quad (2)$$

and the convection boundary condition

$$\hat{\mathbf{n}} \cdot \kappa \nabla T = -h(T - T_a) \quad (3)$$

or

$$\kappa \frac{\partial T}{\partial n} = -h(T - T_a) \quad (4)$$

with  $\hat{\mathbf{n}}$  representing the unit outward normal vector perpendicular to the boundary surface, and  $h$  and  $T_a$  denoting the convective heat transfer coefficient and the ambient temperature, respectively.

Since the PDE in (1) is a parabolic differential equation, the DGTD algorithm cannot be straightforwardly applied to solve it. Instead, (1) has to be transformed to a hyperbolic equation that is able to be written into a conservative form. Motivated by this aim, an intermediate vector variable  $\mathbf{q}(x, y, z, t)$  is introduced, which is given by

$$\mathbf{q}(x, y, z, t) = -\kappa \nabla T. \quad (5)$$

The auxiliary variable  $\mathbf{q}$  actually denotes the heat flux or the rate of heat transfer through a surface per unit time.

With the auxiliary equation (5), the second-order spatial-derivation (the Laplace operator) in (1) can be decreased to a first-order divergence operator. Consequently, (1) can be rewritten as

$$-\nabla \cdot \mathbf{q} + Q = \rho_m c_\rho \frac{\partial T}{\partial t} \quad (6)$$

which is now in a form of conservation.

In this paper, the main focus is to validate the feasibility of DGTD method in solving the transient thermal equation, where the thermal conductivity and the specific heat capacity in (5) and (6) are assumed to be temperature independent. The temperature-dependent situation will be investigated in the future DGTD-based electrical-thermal cosimulation solver, in which the electrical conductivity is also considered to be temperature dependent.

To solve (5) and (6) by the DGTD method, the computational domain  $\Omega$  is first split into a number of nonoverlapping polyhedron elements  $\Omega_i$  (In this paper, tetrahedrons are used to flexibly model the irregular geometries). In each element  $i$ , the nodal basis functions  $\psi(\mathbf{r})$ ,  $\phi(\mathbf{r})$ ,  $\varphi(\mathbf{r})$ , and  $\gamma(\mathbf{r})$  are employed to approximate  $T$ ,  $q_x$ ,  $q_y$ , and  $q_z$ , respectively. By implementing the DG testing over (5) and each component of (6), we have

$$\rho_m c_\rho \int_{\Omega_i} \psi_k^i \frac{\partial T^i}{\partial t} dV = \int_{\Omega_i} \psi_k^i \left( -\nabla \cdot \mathbf{q}^i + Q^i \right) dV \quad (7)$$

$$\int_{\Omega_i} \phi_k^i q_x^i dV = -\kappa \int_{\Omega_i} \phi_k^i \cdot \nabla_x T^i dV \quad (8)$$

$$\int_{\Omega_i} \phi_k^i q_y^i dV = -\kappa \int_{\Omega_i} \phi_k^i \cdot \nabla_y T^i dV \quad (9)$$

$$\int_{\Omega_i} \gamma_k^i q_z^i dV = -\kappa \int_{\Omega_i} \gamma_k^i \cdot \nabla_z T^i dV \quad (10)$$

with  $\nabla_x T = \partial_x T$ ,  $\nabla_y T = \partial_y T$ , and  $\nabla_z T = \partial_z T$ .

Based on the integration by parts and the Gaussian theorem, we have weak formulations of (7)–(10) defined as

$$\rho_m c_\rho \int_{\Omega_i} \psi_k^i \frac{\partial T^i}{\partial t} dV = \int_{\Omega_i} (\mathbf{q}^i \cdot \nabla \psi_k^i + \psi_k^i Q^i) dV - \sum_{f=1}^4 \int_{\partial\Omega_f^i} \psi_k^i \hat{\mathbf{n}}_f^i \cdot \mathbf{q}_f^* dS \quad (11)$$

$$\int_{\Omega_i} \phi_k^i \mathbf{q}_x^i dV = \kappa \int_{\Omega_i} T^i \nabla_x \phi_k^i dV - \kappa \sum_{f=1}^4 \int_{\partial\Omega_f^i} n_{x,f}^i T_f^* \phi_k^i dS \quad (12)$$

$$\int_{\Omega_i} \phi_k^i \mathbf{q}_y^i dV = \kappa \int_{\Omega_i} T^i \nabla_y \phi_k^i dV - \kappa \sum_{f=1}^4 \int_{\partial\Omega_f^i} n_{y,f}^i T_f^* \phi_k^i dS \quad (13)$$

$$\int_{\Omega_i} \gamma_k^i \mathbf{q}_z^i dV = \kappa \int_{\Omega_i} T^i \nabla_z \gamma_k^i dV - \kappa \sum_{f=1}^4 \int_{\partial\Omega_f^i} n_{z,f}^i T_f^* \gamma_k^i dS. \quad (14)$$

It is necessary to mention that the solutions in the adjacent elements are allowed to be discontinuous in the DGTD analysis, thus the values of solutions at the interfaces  $T^*$ ,  $q_x^*$ ,  $q_y^*$ , and  $q_z^*$  involved in the surface integration at the right hand sides of (11)–(14) must be carefully chosen in order to obtain an accurate and unique solution. For hyperbolic systems, the numerical fluxes denoted by  $\mathbf{q}^*$  and  $T^*$  are employed to facilitate the information communication between the neighboring elements. In this paper, we have the following definitions [24]–[26]:

$$\hat{\mathbf{n}}_f^i \cdot \mathbf{q}_f^* = C_{10} (\hat{\mathbf{n}}_f^i \cdot \mathbf{q}^i + \hat{\mathbf{n}}_f^i \cdot \mathbf{q}_f^j) + C_{11} (\hat{\mathbf{n}}_f^i \cdot \mathbf{q}^i - \hat{\mathbf{n}}_f^i \cdot \mathbf{q}_f^j) + C_{12} (T^i - T_f^j) \quad (15)$$

$$T_f^* = C_{20} (T^i + T_f^j) + C_{21} (\hat{\mathbf{n}}_f^i \cdot \mathbf{q}^i - \hat{\mathbf{n}}_f^i \cdot \mathbf{q}_f^j) + C_{22} (T^i - T_f^j) \quad (16)$$

where the superscript  $j$  denotes the neighboring element,  $\hat{\mathbf{n}}_f^i$  represents the unit normal vector at face  $f$ , and the coefficients  $C_{10} = 0.5$ ,  $C_{11} = 0$ ,  $C_{12} = -4$ ,  $C_{20} = 0.5$ ,  $C_{21} = 0$ , and  $C_{22} = 0$ . Specifically, to consider the convection boundary condition in (3) and (4),  $C_{10}$ ,  $C_{12}$ , and  $C_{22}$  are redefined as 0,  $-h$ , and 0.5, respectively.

Next, the unknowns in element  $i$  are approximated by the local nodal basis functions:  $T^i = \sum_{k=1}^{n_T} \psi_k^i(\mathbf{r}) \tilde{T}_k^i(t)$ ,  $q_x^i = \sum_{k=1}^{n_q} \phi_k^i(\mathbf{r}) \tilde{q}_x^i(t)$ ,  $q_y^i = \sum_{k=1}^{n_q} \phi_k^i(\mathbf{r}) \tilde{q}_y^i(t)$ , and  $q_z^i = \sum_{k=1}^{n_q} \gamma_k^i(\mathbf{r}) \tilde{q}_z^i(t)$  with  $n_T^i$  and  $n_q^i$  denoting the number of basis functions for  $T^i$  and  $q_{x,y,z}^i$ , while  $\tilde{T}_k^i(t)$ ,  $\tilde{q}_x^i(t)$ ,  $\tilde{q}_y^i(t)$ , and  $\tilde{q}_z^i(t)$  represent the time-dependent expansion coefficients that are to be determined. By further resorting to (11)–(14) and the definitions of numerical fluxes in (15) and (16), four

semidiscrete matrix equations can be derived. Namely

$$[\bar{\mathbf{M}}_T^i] \frac{\partial \tilde{\mathbf{T}}^i}{\partial t} = [\bar{\mathbf{S}}_x^i] \tilde{\mathbf{q}}_x^i + [\bar{\mathbf{S}}_y^i] \tilde{\mathbf{q}}_y^i + [\bar{\mathbf{S}}_z^i] \tilde{\mathbf{q}}_z^i + \mathbf{Q}^i + \sum_{f=1}^4 \left( [\bar{\mathbf{F}}_{q_x}^{ii}] \tilde{\mathbf{q}}_x^i + [\bar{\mathbf{F}}_{q_y}^{ii}] \tilde{\mathbf{q}}_y^i + [\bar{\mathbf{F}}_{q_z}^{ii}] \tilde{\mathbf{q}}_z^i + [\bar{\mathbf{F}}_{q_x}^{ij}] \tilde{\mathbf{q}}_x^j + [\bar{\mathbf{F}}_{q_y}^{ij}] \tilde{\mathbf{q}}_y^j + [\bar{\mathbf{F}}_{q_z}^{ij}] \tilde{\mathbf{q}}_z^j + [\bar{\mathbf{F}}_T^{ii}] \tilde{\mathbf{T}}^i + [\mathbf{F}_T^{ij}] \tilde{\mathbf{T}}^j \right) \quad (17)$$

$$[\bar{\mathbf{M}}_{q_x}^i] \tilde{\mathbf{q}}_x^i = [\bar{\mathbf{C}}_x^i] \tilde{\mathbf{T}}^i + \sum_{f=1}^4 \left( [\bar{\mathbf{G}}_x^{ii}] \tilde{\mathbf{T}}^i + [\mathbf{G}_x^{ij}] \tilde{\mathbf{T}}^j \right) \quad (18)$$

$$[\bar{\mathbf{M}}_{q_y}^i] \tilde{\mathbf{q}}_y^i = [\bar{\mathbf{C}}_y^i] \tilde{\mathbf{T}}^i + \sum_{f=1}^4 \left( [\bar{\mathbf{G}}_y^{ii}] \tilde{\mathbf{T}}^i + [\mathbf{G}_y^{ij}] \tilde{\mathbf{T}}^j \right) \quad (19)$$

$$[\bar{\mathbf{M}}_{q_z}^i] \tilde{\mathbf{q}}_z^i = [\bar{\mathbf{C}}_z^i] \tilde{\mathbf{T}}^i + \sum_{f=1}^4 \left( [\bar{\mathbf{G}}_z^{ii}] \tilde{\mathbf{T}}^i + [\mathbf{G}_z^{ij}] \tilde{\mathbf{T}}^j \right) \quad (20)$$

where the elements in above matrices are given as

$$\begin{aligned} [\bar{\mathbf{M}}_T^i]_{kl} &= \rho_m c_\rho \int_{\Omega_i} \psi_k^i(\mathbf{r}) \psi_l^i(\mathbf{r}) dV \\ [\bar{\mathbf{M}}_{q_x}^i]_{kl} &= \int_{\Omega_i} \phi_k^i(\mathbf{r}) \phi_l^i(\mathbf{r}) dV \\ [\bar{\mathbf{S}}_x^i]_{kl} &= \int_{\Omega_i} \phi_k^i(\mathbf{r}) \nabla \psi_l^i(\mathbf{r}) dV \\ [\bar{\mathbf{Q}}^i]_k &= \int_{\Omega_i} \phi_k^i(\mathbf{r}) Q dV \\ [\bar{\mathbf{C}}_x^i]_{kl} &= \kappa \int_{\Omega_i} \psi_l^i(\mathbf{r}) \nabla_x \phi_k^i(\mathbf{r}) dV \\ [\bar{\mathbf{F}}_{q_x}^{ii}]_{kl} &= C_{10} \int_{\partial\Omega_{i,f}} \psi_k^i(\mathbf{r}) n_{x,f}^i \phi_l^i(\mathbf{r}) dS \\ [\bar{\mathbf{F}}_{q_x}^{ij}]_{kl} &= C_{10} \int_{\partial\Omega_{i,f}} \psi_k^i(\mathbf{r}) n_{x,f}^i \phi_l^j(\mathbf{r}) dS \\ [\bar{\mathbf{F}}_T^{ii}]_{kl} &= C_{12} \int_{\partial\Omega_{i,f}} \psi_k^i(\mathbf{r}) \psi_l^i(\mathbf{r}) dS \\ [\bar{\mathbf{F}}_T^{ij}]_{kl} &= -C_{12} \int_{\partial\Omega_{i,f}} \psi_k^i(\mathbf{r}) \psi_l^j(\mathbf{r}) dS \\ [\bar{\mathbf{G}}_x^{ii}]_{kl} &= \kappa (C_{20} + C_{22}) \int_{\partial\Omega_{i,f}} \phi_k^i(\mathbf{r}) n_{x,f}^i \psi_l^i(\mathbf{r}) dS \\ [\bar{\mathbf{G}}_x^{ij}]_{kl} &= \kappa (C_{20} - C_{22}) \int_{\partial\Omega_{i,f}} \phi_k^i(\mathbf{r}) n_{x,f}^i \psi_l^j(\mathbf{r}) dS. \end{aligned} \quad (21)$$

For other elements in  $[\bar{\mathbf{S}}_y^i]$ ,  $[\bar{\mathbf{S}}_z^i]$ ,  $[\bar{\mathbf{C}}_y^i]$ ,  $[\bar{\mathbf{C}}_z^i]$ ,  $[\bar{\mathbf{F}}_{q_y}^{ii}]$ ,  $[\bar{\mathbf{F}}_{q_z}^{ii}]$ ,  $[\bar{\mathbf{G}}_y^{ii}]$ ,  $[\bar{\mathbf{G}}_z^{ii}]$ ,  $[\bar{\mathbf{G}}_y^{ij}]$ , and  $[\bar{\mathbf{G}}_z^{ij}]$ , their definitions have similar expressions to those in the  $x$ -direction.

In this paper, each unknown in every tetrahedron is approximated by four nodal basis functions, namely,  $n_T^i = 4$  and  $n_q^i = 4$ . Therefore, the dimension of the matrix equation to be solved is 4 by 4. As a result, the computational cost for the matrix factorization is negligible.

To keep an explicit time marching scheme, the first-order time-derivative in (17) is discretized by the forward Euler method. For the explicit scheme, the Courant–Friedrichs–Lewy condition must be satisfied to ensure stability. In this

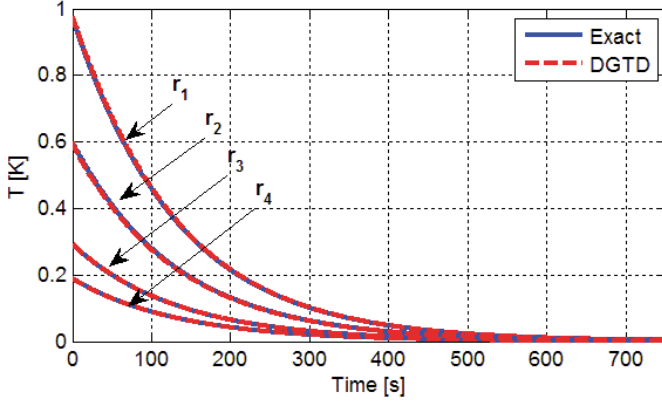


Fig. 1. Calculated temperature  $T$  by DGTD at  $\mathbf{r}_1 = 0.252\hat{x} + 0.249\hat{y} + 0.284\hat{z}$ ,  $\mathbf{r}_2 = 0.255\hat{x} + 0.231\hat{y} + 0.103\hat{z}$ ,  $\mathbf{r}_3 = 0.232\hat{x} + 0.255\hat{y} + 0.048\hat{z}$ , and  $\mathbf{r}_4 = 0.04\hat{x} + 0.255\hat{y} + 0.141\hat{z}$ . For comparison, the analytical results (blue curve) obtained from (23) are given as well.

paper, the time-stepping size for the  $i$ th element is determined in terms of the following condition:

$$\Delta t \leq \alpha \cdot \min \left\{ l_{\min}^2 / [\kappa / \rho c_p] \right\} \quad (22)$$

with  $\alpha$  depending on the order of basis function and the type of spatial discretization.

### III. NUMERICAL RESULTS

In this section, several representative examples are provided to verify and validate the accuracy of the proposed algorithm.

#### A. Rectangular Silicon Brick

In order to validate the feasibility and accuracy of the DGTD algorithm subjected to different boundary conditions, a rectangular silicon brick is studied. The dimensions of the brick in the  $x$ -,  $y$ -, and  $z$ -directions are given by  $L_x = 0.5$  m,  $L_y = 0.5$  m, and  $L_z = 0.5$  m, respectively. First, the DGTD algorithm is benchmarked with the Dirichlet boundary condition:  $T(x, y, z, t)|_{x=0} = 0$ ,  $T(x, y, z, t)|_{x=L_x} = 0$ ,  $T(x, y, z, t)|_{z=0} = 0$ ,  $T(x, y, z, t)|_{z=L_z} = 0$ , and the initial solution  $T(x, y, z, t)|_{t=0} = \sin(\pi x/L_x)\sin(\pi z/L_z)$ . Correspondingly, we have the analytical solution described as

$$T(x, y, z, t) = \sin\left(\frac{\pi x}{L_x}\right) \sin\left(\frac{\pi z}{L_z}\right) \times \exp\left[-\frac{\kappa \pi^2 t}{\rho c_p} \left(\frac{1}{L_x^2} + \frac{1}{L_z^2}\right)\right] \quad (23)$$

with  $\kappa = 160$  W/[m.K],  $\rho = 2300$  kg/m<sup>3</sup>, and  $c_p = 730$  J/[kg.K] in this simulation.

After the DGTD analysis, the computed temperature profiles at four different points are plotted versus the time as shown in Fig. 1. It is noted that the numerical results are in good consistence with the analytical references. In Fig. 2, the 3-D temperature distribution at  $t = 12.4$  s is also given. For comparison, the analytical reference is provided again. Very good agreement between the numerical results and the reference solutions is observed. To have a better clarification, the  $L_2$  norm errors at the four observation points are calculated

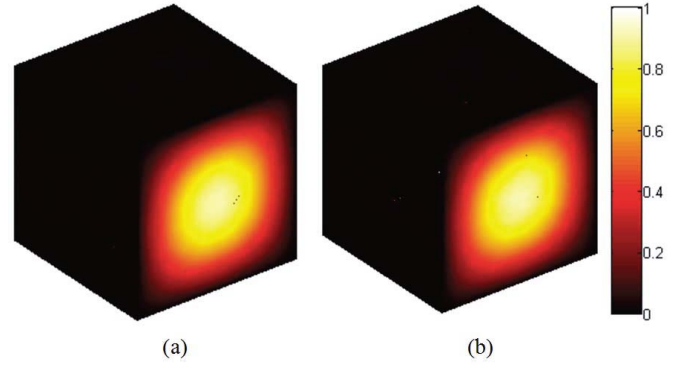


Fig. 2. 3-D transient temperature (K) obtained by (a) DGTD simulation and (b) analytical formula (23).

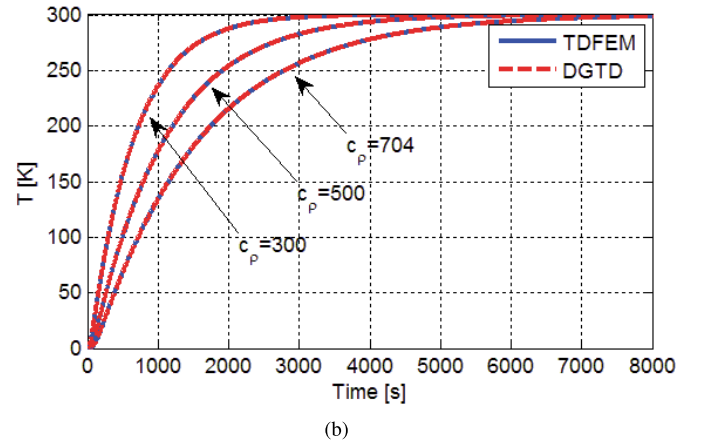
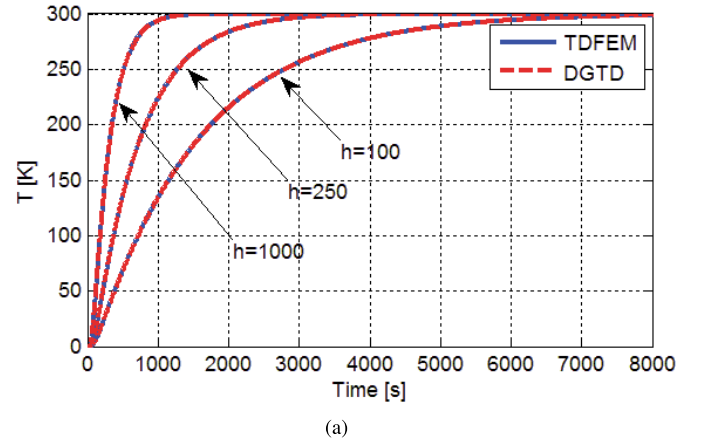


Fig. 3. Calculated temporal temperature at  $\mathbf{r} = 0.185\hat{x} + 0.18\hat{y} + 0.256\hat{z}$  for (a) different convective heat transfer coefficients and (b) specific heat capacity. For comparison, the results from the TDFEM are given as well.

as  $8.41 \times 10^{-3}$ ,  $9.78 \times 10^{-3}$ ,  $2.14 \times 10^{-3}$ , and  $3.22 \times 10^{-3}$ . Thus, the accuracy of DGTD for the Dirichlet boundary condition is successfully demonstrated. In the DGTD method, the implementation of Dirichlet boundary condition is similar to that in the FEM, for nodes at the Dirichlet boundary, the unknown coefficients of the corresponding nodal basis are explicitly given. Thus, only unknowns not over the Dirichlet boundary condition are to be solved.

In practical thermal systems, the convective boundary condition must be considered since air cooling is popularly

TABLE I  
GEOMETRY INFORMATION AND EQUIVALENT THERMAL PARAMETERS

Layer	Dimension (mm <sup>3</sup> )	Material	$\kappa$ (W/[m·K])	$\rho$ (kg/m <sup>3</sup> )	$c_p$ (J/[kg·K])
TIM	10 × 10 × 0.75	epoxy	1.6	3100	610
Die	10 × 10 × 1.25	Si	130	2329	700
Microbump-1	10 × 10 × 0.25	SnAg & epoxy	⊥0.9, //0.6	1547	1381
Interposer	30 × 30 × 0.5	Cu & Si	⊥170, //25	3197	583
Microbump-2	30 × 30 × 0.75	SnAg & epoxy	⊥0.9, //0.6	1547	1381
Package	48 × 48 × 4.5	FR4	0.3	1900	1369

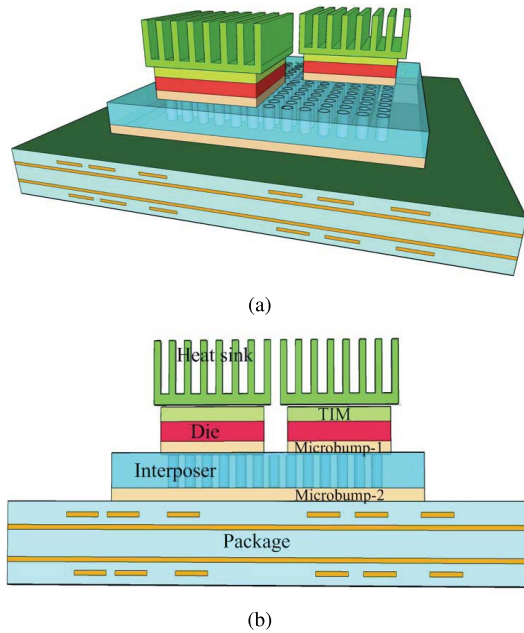


Fig. 4. (a) 3-D view of the integrated system. (b) Cross-sectional view of the structure.

employed to cool down the integrated chips. To achieve this purpose, the six boundary surfaces of the above brick are imposed with the convective boundary.

We first suppose that the parameters including the thermal conductivity  $\kappa$ , the mass density  $\rho$ , the specific heat capacity  $c_p$ , and the ambient temperature  $T_a$  are fixed to 135 W/[m·K], 2330 kg/m<sup>3</sup>, 704 J/[kg·K], and 300 K, respectively, while the convective heat transfer coefficient  $h$  is set to be different values. In Fig. 3(a), the temporal temperature at  $\mathbf{r} = 0.185\hat{x} + 0.18\hat{y} + 0.256\hat{z}$  is provided. As can be seen, the temperature increases faster for larger convection coefficient. For comparison, the results from the time domain FEM (TDFEM) are given. As can be seen, obvious consistencies are reached. The  $L_2$  norm errors corresponding to  $h = 100$ , 250, and 1000 are  $1.56 \times 10^{-4}$ ,  $2.75 \times 10^{-4}$ , and  $5.84 \times 10^{-4}$ , respectively.

Next, the convective heat transfer coefficient  $h$  is fixed to be 100 W/[m<sup>2</sup>·K], and the specific heat capacity  $c_p$  is varied. In Fig. 3(b), the temperature  $T$  at the same point is shown as the function of time. As expected, the larger specific heat capacity causes the slower temperature rise since it needs more energy to raise the same amount of temperature. The numerical results agree very well with the TDFEM references, and the  $L_2$  norm

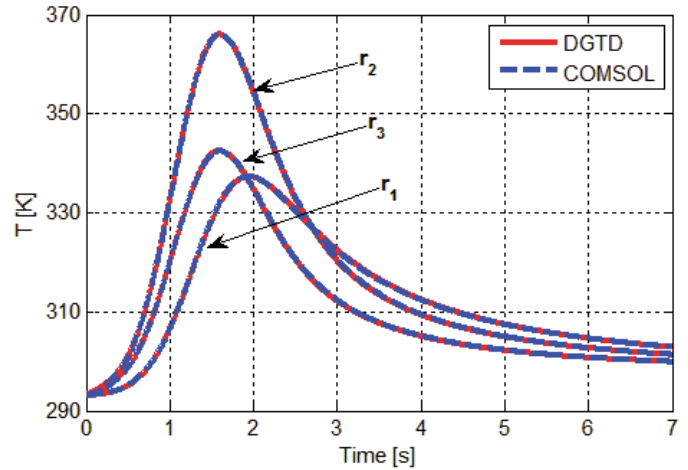


Fig. 5. DGTD calculated temperature at three observation points  $\mathbf{r}_1$ ,  $\mathbf{r}_2$ , and  $\mathbf{r}_3$ . For verification purposes, the results simulated by COMSOL are also given.

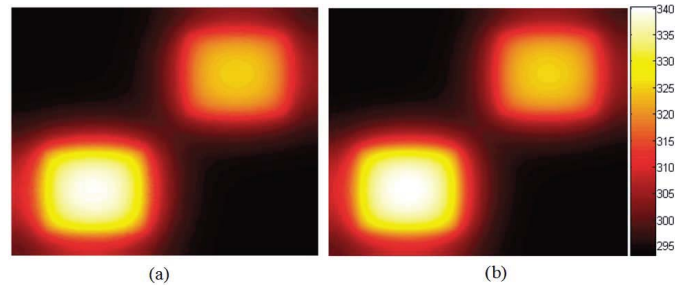


Fig. 6. Snapshot of the temperature profile (K) at the top surface of the interposer at  $t = 2$  s. (a) Numerical result by the DGTD method. (b) Reference by COMSOL.

errors corresponding to  $c_p = 300$ , 500, and 700 are  $1.02 \times 10^{-4}$ ,  $1.52 \times 10^{-4}$ , and  $1.56 \times 10^{-4}$ , respectively. Thereby, the accuracy of proposed DGTD method has been validated for both Dirichlet and convection boundary conditions.

Here, the number of mesh elements is 4530, the CPU time of each time marching step is around 0.0052 s, and the peak memory cost is around 0.01 GB.

### B. 3-D Integrated System With Equivalent Thermal Parameters

In this example, a 3-D integration structure shown in Fig. 4 is investigated, where the geometrical details and material properties are given in Table I. Instead of directly considering the physical presence of TSVs and ball grid array,

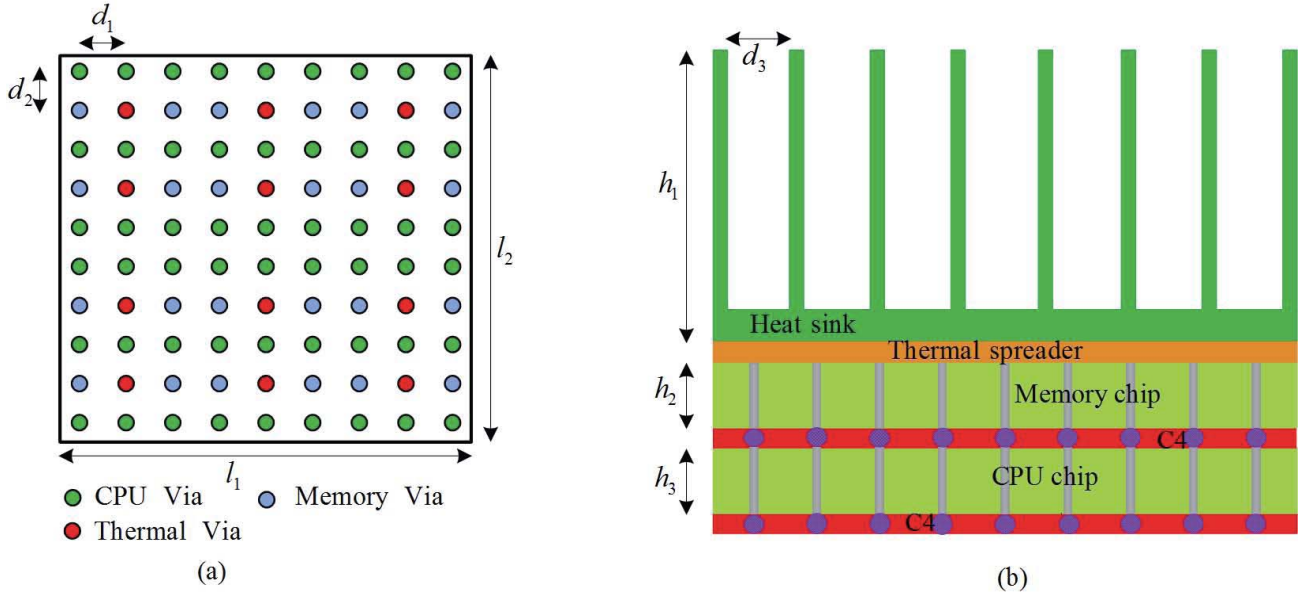


Fig. 7. Geometrical details of the investigated 3-D package. (a) Distribution of different vias. (b) Cross-sectional view of the package. The geometrical parameters are given as  $l_1 = 12$  mm,  $l_2 = 12$  mm,  $d_1 = 1.25$  mm,  $d_2 = 1.25$  mm,  $d_3 = 1.95$  mm,  $h_1 = 7$  mm,  $h_2 = 0.5$  mm, and  $h_3 = 0.5$  mm. The thickness of thermal spreader is 0.2 mm as well as C4.

TABLE II  
MATERIAL PROPERTIES REQUIRED BY THE THERMAL ANALYSIS

...	$\kappa$ W/[m·K]	$c_m$ J/[kg·K]	$\rho$ kg/m <sup>3</sup>
Thermal Spreader	400	385	8933
Heat Sink	220	896	2707
Chip Die	135	704	2330
TSV	400	385	8933
C4	50	180	9290

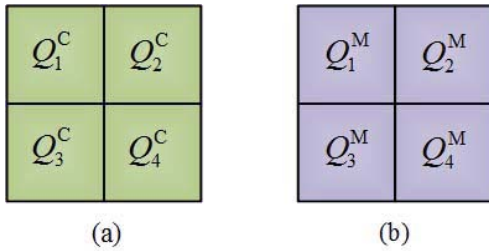


Fig. 8. Power map over (a) CPU die and (b) memory die, where  $Q_1^C = 20Q_c$ ,  $Q_2^C = 30Q_c$ ,  $Q_3^C = 35Q_c$ ,  $Q_4^C = 25Q_c$ ,  $Q_1^M = 60Q_m$ ,  $Q_2^M = 70Q_m$ ,  $Q_3^M = 65Q_m$ , and  $Q_4^M = 63Q_m$  with  $Q_c = \|\cos(2\pi y/3l_1)\|$  and  $Q_m = \|\cos(3\pi y/2l_1)\|$ .

the thermal effects of TSVs in the interposer and ball grid array in the microbump layer are equivalently replaced by revising the thermal parameters of materials in the corresponding layer [27]. In this way, the homogeneous meshes can be employed to model this structure, which consequently results in only 15 208 elements. The power consumption on dies is a Gaussian pulse defined by  $Q = Q_0 \exp[-(t - 1.2)^2/0.36]$  W/m<sup>3</sup> with  $Q_0 = 3.6 \times 10^8$  on the first die and  $Q_0 = 2.4 \times 10^8$  on the second die. The isotherm boundary of 298.15 K is applied to the top surface of the TIM as the heat

sink, while the convection boundary with  $h = 5$  W/[m<sup>2</sup> · K] is applied to the remaining surfaces of the package.

To verify the accuracy of the proposed algorithm, the transient temperature at three observation points  $\mathbf{r}_1$ ,  $\mathbf{r}_2$ , and  $\mathbf{r}_3$  with  $\mathbf{r}_1 = 0.015\hat{x} + 0.015\hat{y} + 0.007\hat{z}$ ,  $\mathbf{r}_2 = 0.017\hat{x} + 0.017\hat{y} + 0.008125\hat{z}$ , and  $\mathbf{r}_3 = 0.031\hat{x} + 0.031\hat{y} + 0.008125\hat{z}$  located at the interposer layer, the center of first and second dies, respectively, are computed as shown in Fig. 5. For comparison, the solutions simulated by the commercial software COMSOL [28] are also presented. As can be seen, the calculated numerical results agree very well with the references. For further verification, the temperature distribution over the top surface of the interposer at  $t = 2$  s is calculated and plotted in Fig. 6. As can be seen, the calculated result from DGTD algorithm associates with the reference from the COMSOL simulation [28].

In this example, the CPU time of each time-step is 0.019 s, and the memory cost is around 0.06 GB.

### C. 3-D Integration Package and Interconnect

To further demonstrate the capability of the proposed algorithm for analyzing complicated multiscale systems, a 3-D integrated circuit package with vertically stacked-up chips connected by TSVs is studied, as shown in Fig. 7. This module is composed of one CPU chip and one memory die, 12 thermal vias, 54 TSVs in the CPU layer, 24 TSVs in the memory layer, a thermal spreader, and a heat sink. In Table II, the thermal equation required parameters are listed. Unlike the second example, all the geometrical elements here are modeled rigorously without using the equivalent thermal parameters. It is supposed that the convection boundary is applied at the surface of the heat sink with  $h = 50$  W/[m<sup>2</sup> · K], and other surfaces are assumed to be adiabatic



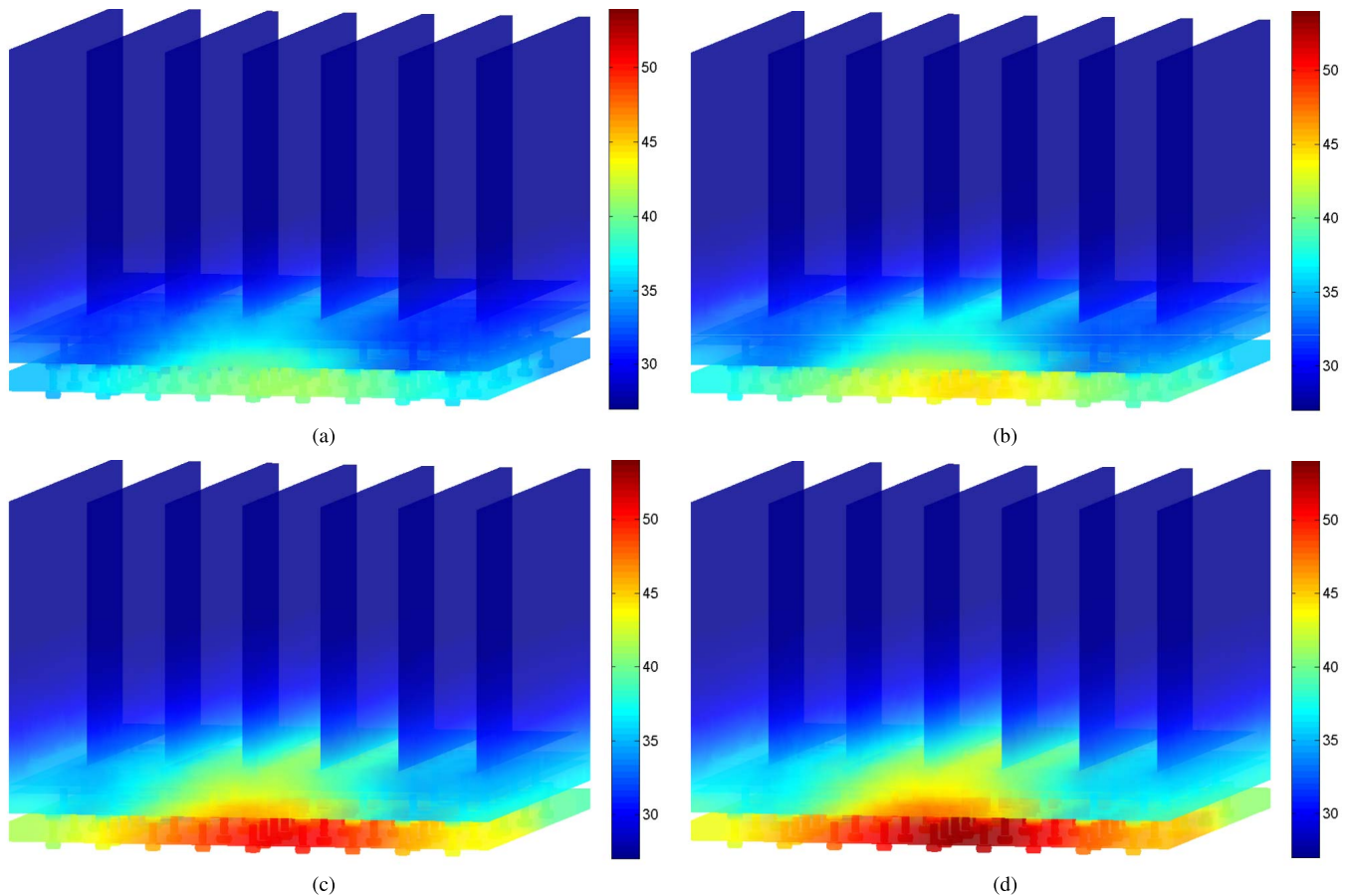


Fig. 9. DGTD calculated temperature distributions ( $^{\circ}\text{C}$ ) of the 3-D integrated circuit at (a)  $t = 0.0138$  s, (b)  $t = 0.02$  s, (c)  $t = 0.0242$  s, and (d)  $t = 0.027$  s.

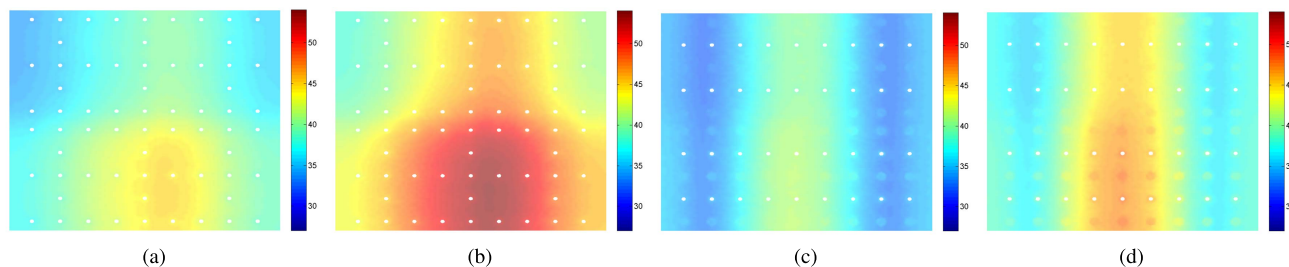


Fig. 10. (a) and (b) Temperature profiles ( $^{\circ}\text{C}$ ) over the bottom surface of the CPU die at  $t = 0.02$  s and  $t = 0.027$  s, respectively. (c) and (d) Temperature profiles over the bottom surface of the memory die at  $t = 0.02$  s and  $t = 0.027$  s, respectively.

(The convective heat transfer coefficient  $h = 0 \text{ W}/[\text{m}^2 \cdot \text{K}]$ ). The heat power consumptions of the CPU and memory dies are described in Fig. 8, while a 50-W impressed heat source is placed over the thermal spreader. Totally, 469 220 strongly inhomogeneous tetrahedrons are generated, which results in 7 507 520 unknowns. Even though there are more than seven million unknowns, in the DGTD analysis, the dimension of the matrix equation for factorization is 4 by 4 since the DGTD method in this paper solves the whole computational domain in an element-by-element scheme. Thus, it is free of issues encountered in the FEM such as factorization of a very large matrix (the dimension of the global matrix is a few millions) that could be seriously ill-conditioned due to the very inhomogeneous mesh cells.

In Fig. 9, the 3-D temperature profiles at  $t = 0.0138$  s,  $t = 0.02$  s,  $t = 0.0242$  s, and  $t = 0.027$  s obtained from the proposed DGTD algorithm are provided. The 2-D temperatures at the bottom surfaces of the CPU die and memory die at  $t = 0.02$  s and  $t = 0.027$  s are plotted in Fig. 10. It is interestingly noted that the temperature of the memory die raises slowly compared to the CPU die although the power consumption in the memory die is higher, which is attributed to the memory die attached with the thermal spreader so that the generated heat can be transferred to the heat sink.

Finally, consider that the above heat sources are modulated by a pulse  $G_0(t)$  shown in Fig. 11. The transient temperature variations at different positions over the chip

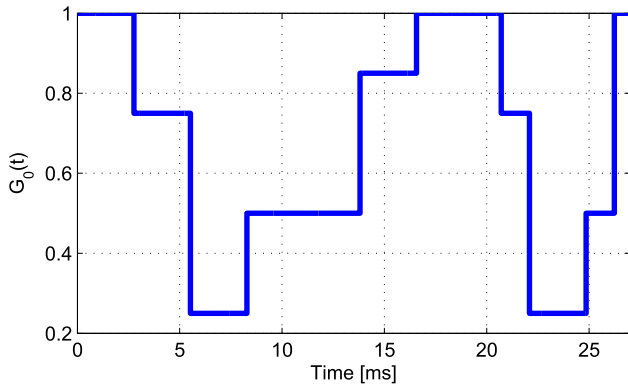
Fig. 11. Pulse  $G_0(t)$  used to modulate the heat source.

TABLE III  
CORRESPONDING SPATIAL COORDINATES (mm)  
FOR THE CURVES IN FIG. 12

...	$r_1$	$r_2$	$r_3$	$r_4$	$r_5$	$r_6$
x	0.1934	-4.8852	-5.0297	-5.0297	-3.5006	-1.4872
y	0.0013	0.0007	-3.0952	-3.0952	-2.8667	4.8062
z	0.3547	0.1693	0.3022	0.3022	0.9162	0.9166

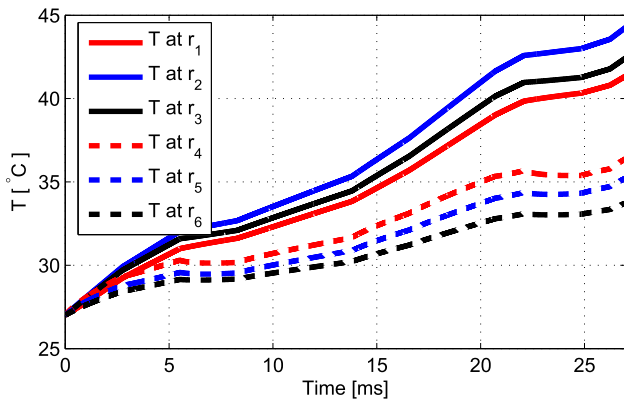


Fig. 12. Transient temperature profiles (°C) at different positions listed in Table II.

die and memory die listed in Table III are plotted in Fig. 12.

For this example, the CPU time of each time marching step is around 0.7 s, and the peak memory cost is around 1.52 GB.

#### IV. CONCLUSION

A DGTD algorithm is developed in this paper for analyzing the heat transfers in 3-D integrated circuits and packages. To solve the parabolic heat equation by the DGTD method, an auxiliary vector named heat flux is introduced that degenerates the parabolic one to a hyperbolic equation. Due to the local operation of DGTD, the whole computational domain can be solved in an element-by-element scheme. Thus, it is free of issues such as the factorization of a huge matrix equation that is usually ill-conditioned due to multiscale meshes. The proposed algorithm is verified both analytically and numerically, as well as its capability to handle multiscale structures.

#### REFERENCES

- [1] R. R. Tummala, "SOP: What is it and why? A new microsystem-integration technology paradigm-Moore's law for system integration of miniaturized convergent systems of the next decade," *IEEE Trans. Adv. Packag.*, vol. 27, no. 2, pp. 241–249, May 2004.
- [2] T. Sudo, H. Sasaki, N. Masuda, and J. L. Drewniak, "Electromagnetic interference (EMI) of system-on-package (SOP)," *IEEE Trans. Adv. Packag.*, vol. 27, no. 2, pp. 304–314, May 2004.
- [3] J. U. Knickerbocker *et al.*, "3-D silicon integration and silicon packaging technology using silicon through-vias," *IEEE J. Solid-State Circuits*, vol. 41, no. 8, pp. 1718–1725, Aug. 2006.
- [4] A. Jain, R. E. Jones, R. Chatterjee, and S. Pozder, "Analytical and numerical modeling of the thermal performance of three-dimensional integrated circuits," *IEEE Trans. Compon. Packag. Technol.*, vol. 33, no. 1, pp. 56–63, Mar. 2010.
- [5] Y. Shao, Z. Peng, and J. F. Lee, "Thermal analysis of high-power integrated circuits and packages using nonconformal domain decomposition method," *IEEE Trans. Compon., Packag., Manuf. Technol.*, vol. 3, no. 8, pp. 1321–1331, Aug. 2013.
- [6] Y. Shao, Z. Peng, and J.-F. Lee, "Thermal-aware DC IR-drop co-analysis using non-conformal domain decomposition methods," *Proc. Roy. Soc. A*, vol. 468, pp. 1652–1675, Feb. 2012.
- [7] J. Xie and M. Swaminathan, "Electrical-thermal co-simulation of 3D integrated systems with micro-fluidic cooling and Joule heating effects," *IEEE Trans. Compon., Packag., Manuf. Technol.*, vol. 1, no. 2, pp. 234–246, Feb. 2011.
- [8] J. Xie and M. Swaminathan, "System-level thermal modeling using nonconformal domain decomposition and model-order reduction," *IEEE Trans. Compon., Packag., Manuf. Technol.*, vol. 4, no. 1, pp. 66–76, Jan. 2014.
- [9] Z. Liu, S. Swarup, S. X.-D. Tan, H.-B. Chen, and H. Wang, "Compact lateral thermal resistance model of TSVs for fast finite-difference based thermal analysis of 3-D stacked ICs," *IEEE Trans. Comput.-Aided Design Integr. Circuits Syst.*, vol. 33, no. 10, pp. 1490–1502, Oct. 2014.
- [10] S. Ghalambor, D. Agonafer, and A. Haji-Sheikh, "Analytical thermal solution to a nonuniformly powered stack package with contact resistance," *J. Heat Transf.*, vol. 135, no. 11, pp. 111015-1–111015-9, Nov. 2013.
- [11] L. Choobineh and A. Jain, "An explicit analytical model for rapid computation of temperature field in a three-dimensional integrated circuit (3D IC)," *Int. J. Thermal Sci.*, vol. 87, pp. 103–109, Jan. 2015.
- [12] T. Lu and J.-M. Jin, "Transient electrical-thermal analysis of 3-D power distribution network with FETI-enabled parallel computing," *IEEE Trans. Compon., Packag., Manuf. Technol.*, vol. 4, no. 10, pp. 1684–1695, Oct. 2014.
- [13] T. Lu and J.-M. Jin, "Electrical-thermal co-simulation for DC IR-drop analysis of large-scale power delivery," *IEEE Trans. Compon., Packag., Manuf. Technol.*, vol. 4, no. 2, pp. 323–331, Feb. 2014.
- [14] T. J. Lu and J.-M. Jin, "Thermal-aware high-frequency characterization of large-scale through-silicon-via structures," *IEEE Trans. Compon., Packag., Manuf. Technol.*, vol. 4, no. 6, pp. 1015–1025, Jun. 2014.
- [15] R. Zhang, M. R. Stan, and K. Skadron, "HotSpot 6.0: Validation, acceleration and extension." Univ. Virginia, Charlottesville, VA, USA, Tech. Rep. CS-2015-04, 2015.
- [16] *HotSpot 6.0*, accessed on 2015. [Online]. Available: <http://lava.cs.virginia.edu/HotSpot/index.htm>
- [17] J. S. Hesthaven and T. Warburton, *Nodal Discontinuous Galerkin Methods*. Berlin, Germany: Springer, 2008.
- [18] A. Zjajo, N. van der Meijs, and R. van Leuken, "Thermal analysis of 3D integrated circuits based on discontinuous Galerkin finite element method," in *Proc. Int. Symp. Quality Electron. Design*, Sep. 2012, pp. 117–122.
- [19] S. D. Gedney, J. C. Young, T. C. Kramer, and J. A. Roden, "A discontinuous Galerkin finite element time-domain method modeling of dispersive media," *IEEE Trans. Antennas Propag.*, vol. 60, no. 4, pp. 1969–1977, Apr. 2012.
- [20] P. Li and L. J. Jiang, "Integration of arbitrary lumped multiport circuit networks into the discontinuous Galerkin time-domain analysis," *IEEE Trans. Microw. Theory Techn.*, vol. 61, no. 7, pp. 2525–2534, Jul. 2013.
- [21] K. Sankaran, "Accurate domain truncation techniques for time-domain conformal methods," Ph.D. dissertation, Dept. Inf. Technol. Elect. Eng., ETH Zurich, Zürich, Switzerland, 2007.
- [22] M. Dumbser, M. Käser, and E. F. Toro, "An arbitrary high-order discontinuous Galerkin method for elastic waves on unstructured meshes—II. The three-dimensional isotropic case," *Geophys. J. Int.*, vol. 171, pp. 695–717, Apr. 2007.

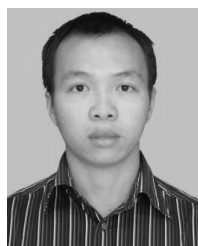


- [23] S. Dosopoulos and J. F. Lee, "Interconnect and lumped elements modeling in interior penalty discontinuous Galerkin time-domain methods," *J. Comput. Phys.*, vol. 229, pp. 8521–8536, Aug. 2010.
- [24] L. Evans, *Partial Differential Equations*. Philadelphia, PA, USA: American Society of Mathematics, 2000.
- [25] C. Fletcher, *Computational Techniques for Fluid Dynamics*. Berlin, Germany: Springer-Verlag, 1991.
- [26] B. Cockburn, "Discontinuous Galerkin methods for convection-dominated problems," in *High-Order Methods for Computational Physics*, vol. 9. Berlin, Germany: Springer, 1999, pp. 69–224.
- [27] J. H. Lau and T. G. Yue, "Effects of TSVs (through-silicon vias) on thermal performances of 3D IC integration system-in-package (SiP)," *Microelectron. Rel.*, vol. 52, no. 11, pp. 2660–2669, 2012.
- [28] *COMSOL Multiphysics 5.2*, accessed on 2016. [Online]. Available: <https://br.comsol.com/>



**Min Tang** (M'09) was born in 1980. He received the B.S. degree in electronic engineering from Northwestern Polytechnical University, Xi'an, China, in 2001, the M.S. degree in electrical engineering from Xi'an Jiao Tong University, Xi'an, in 2004, and the Ph.D. degree in electronic engineering from Shanghai Jiao Tong University, Shanghai, China, in 2007.

He was a Post-Doctoral Research Fellow with the University of Hong Kong, Hong Kong, from 2010 to 2012. Since 2007, he has been a Faculty Member with Shanghai Jiao Tong University, where he is currently an Associate Professor with the Department of Electronic Engineering. His current research interests include modeling and simulation of high-speed interconnects, CAD of very large-scale integration circuits, and computational electromagnetics.



**Ping Li** (S'12–M'15–SM'16) is currently pursuing the Ph.D. degree with the Center of Electromagnetics and Optics, University of Hong Kong, Hong Kong.

He has authored over 10 journal papers in the IEEE TRANSACTIONS ON MICROWAVE THEORY AND TECHNIQUES, the IEEE TRANSACTIONS ON ANTENNAS AND PROPAGATION, the IEEE TRANSACTIONS ON ELECTROMAGNETIC AND COMPATIBILITY, the IEEE TRANSACTIONS ON COMPONENTS, PACKAGING, AND MANUFACTURING TECHNOLOGIES, and so on. His current research interests include the near-field-to-far-field transformation techniques, phaseless equivalent source reconstruction methods, discontinuous Galerkin time-domain method, and uncertainty quantification for large-scale electromagnetic systems.

Mr. Li was a recipient of the Postgraduate Engineering Fellowship for outstanding academic performance in 2010 and the Best Student Paper Award in the 12th International Workshop on Finite Elements for Microwave Engineering. He was listed in Marquis Who's Who in the World, 32nd Edition, in 2015. His paper was selected as the Finalist Paper in the 29th International Review of Progress in Applied Computational Electromagnetics and the 2014 International Symposium on Electromagnetic Compatibility. He served as a Reviewer of the IEEE TRANSACTIONS ON MICROWAVE THEORY AND TECHNIQUES, the IEEE TRANSACTIONS ON ANTENNAS AND PROPAGATION, the IEEE ANTENNAS AND WIRELESS PROPAGATION LETTERS, the PROCEEDINGS OF IEEE, *Journal of Electromagnetic Waves and Applications*, *Journal of Applied Computational Electromagnetics*, *PIER*, *IET*, and so on. He is the Guest Editor of the *International Journal of Antenna and Propagation*.

Mr. Li was a recipient of the Postgraduate Engineering Fellowship for outstanding academic performance in 2010 and the Best Student Paper Award in the 12th International Workshop on Finite Elements for Microwave Engineering. He was listed in Marquis Who's Who in the World, 32nd Edition, in 2015. His paper was selected as the Finalist Paper in the 29th International Review of Progress in Applied Computational Electromagnetics and the 2014 International Symposium on Electromagnetic Compatibility. He served as a Reviewer of the IEEE TRANSACTIONS ON MICROWAVE THEORY AND TECHNIQUES, the IEEE TRANSACTIONS ON ANTENNAS AND PROPAGATION, the IEEE ANTENNAS AND WIRELESS PROPAGATION LETTERS, the PROCEEDINGS OF IEEE, *Journal of Electromagnetic Waves and Applications*, *Journal of Applied Computational Electromagnetics*, *PIER*, *IET*, and so on. He is the Guest Editor of the *International Journal of Antenna and Propagation*.



**Junfa Mao** (M'92–SM'98–F'12) was born in 1965. He received the B.S. degree in radiation physics from the University of Science and Technology of the National Defense, Changsha, China, in 1985, the M.S. degree in experimental nuclear physics from the Shanghai Institute of Nuclear Research, Shanghai, China, in 1988, and the Ph.D. degree in electronic engineering from Shanghai Jiao Tong University, Shanghai, in 1992.

He was a Visiting Scholar with the Chinese University of Hong Kong, Hong Kong, from 1994 to

1995, and a Post-Doctoral Researcher with the University of California, Berkeley, CA, USA, from 1995 to 1996. Since 1992, he has been a Faculty Member with Shanghai Jiao Tong University, where he is currently a Chair Professor and the Dean of the School of Electronic Information and Electrical Engineering. He has authored or coauthored more than 250 journal papers (including more than 110 IEEE journal papers) and 150 international conference papers. His current research interests include the interconnect and package problem of integrated circuits and systems, analysis, and design of microwave circuits.

Dr. Mao was a member of the IEEE Microwave Theory and Techniques Society Fellow Evaluation Committee, a member of the 2015 IEEE Fellow Committee, and the Founder and the 2007–2009 Chair of the IEEE Shanghai Section. He was a recipient of the National Natural Science Award of China in 2004, the National Technology Invention Award of China in 2008, the National Science and Technology Advancement Award of China in 2012, and the Best Paper Award of the 2008 Symposium of APEMC. He is a Chief Scientist of the National Basic Research Program of China, a Project Leader of the National Science Foundation for Creative Research Groups of China, a Cheung Kong Scholar of the Ministry of Education, China, an Associate Director of the Microwave Society of China Institute of Electronics, and the 2009–2016 Chair of the IEEE MTT-S Shanghai Chapter.



**Yilin Dong** (S'14) received the B.E. degree in electromagnetic field and radio technology from Xidian University, Xi'an, China, in 2014. She is currently pursuing the Ph.D. degree in electronic science and technology with Shanghai Jiao Tong University, Shanghai, China.

Her current research interests include computational electromagnetics, electrical-thermal cosimulation, and multiphysics in integrated systems.



**Li Jun Jiang** (S'01–M'04–SM'13) received the B.S. degree in electrical engineering from the Beijing University of Aeronautics and Astronautics, Beijing, China, in 1993, the M.S. degree from Tsinghua University, Beijing, in 1996, and the Ph.D. degree from the University of Illinois at Urbana–Champaign, Champaign, IL, USA, in 2004.

From 1996 to 1999, he was an Application Engineer with Hewlett-Packard Company. He served as a Scientific Consultant with the Hong Kong Applied Science and Technology Research Institute Company Limited, Shatin, Hong Kong, from 2010 to 2011, and has been a Panelist with the Expert Review Panel of the Hong Kong Research and Development Center for Logistics and Supply Chain Management Enabling Technologies since 2013. He has also been a Senior Visiting Professor with Tsinghua University since 2013. Since 2004, he has been a Post-Doctoral Researcher, a Research Staff Member, and a Senior Engineer with the IBM Thomas J. Watson Research Center, Yorktown Heights, NY, USA. Since 2009, he has also been an Associate Professor with the Department of Electrical and Electronic Engineering, University of Hong Kong, Hong Kong.

Dr. Jiang was a recipient of the IEEE MTT Graduate Fellowship Award in 2003 and the Y. T. Lo Outstanding Research Award in 2004. He is an Associate Editor of the IEEE TRANSACTIONS ON ANTENNAS AND PROPAGATION, the Associate Editor of *Progress in Electromagnetics Research*, the Associate Guest Editor of the PROCEEDINGS OF IEEE Special Issue in 2011–2012, an IEEE AP-S Member, an IEEE MTT-S Member, an IEEE EMC-S Member, an ACES Member, and a member of the Chinese Computational Electromagnetics Society. He was the Semiconductor Research Cooperation Industrial Liaison for several academic projects. He was the TPC Chair of the 7th International Conference on Nanophotonics/the 3rd Conference on Advances in Optoelectronics and Micro/Nano Optics, the TPC Co-Chair of the 12th International Workshop on Finite Elements for Microwave Engineering, the Co-Chair of 2013 International Workshop on Pulsed Electromagnetic Field at Delft, The Netherlands, and the General Chair of the 2014 IEEE 14th HK AP/MTT Postgraduate Conference. He has been the elected TPC Member of the IEEE EPEP since 2014 and the TPC Member of the IEEE EDAPS since 2010, and was the TPC Member of the 2013 IEEE ICMTCE, the Scientific Committee Member of the 2010 IEEE SMEE, and the Special Session Organizers of the IEEE EDAPS, the IEEE EMC, ACES, AP-RASC, and *PIERS*. He was the Co-organizer of the HKU Computational Science and Engineering Workshops in 2010–2012, and has been the TC-9 and TC-10 Member of the IEEE EMC-S since 2011, and the Session Chair of many international conferences. He also serves as a Reviewer of the IEEE transactions on several topics and other primary electromagnetics- and microwave-related journals. He has been collaboratively involved with many international researchers.



**Hakan Bağcı** (S'98–M'07–SM'14) received the B.S. degree in electrical and electronics engineering from Bilkent University, Ankara, Turkey, in 2001, and the M.S. and Ph.D. degrees in electrical and computer engineering from the University of Illinois at Urbana–Champaign (UIUC), Urbana, IL, USA, in 2003 and 2007, respectively.

From 1999 to 2001, he was an Undergraduate Researcher with the Computational Electromagnetics Group, Bilkent University. From 2001 to 2006, he was a Research Assistant with the Center for

Computational Electromagnetics and Electromagnetics Laboratory, UIUC. From 2007 to 2009, he was a Research Fellow with the Radiation Laboratory, University of Michigan, Ann Arbor, MI, USA. In 2009, he joined the Division of Physical Sciences and Engineering, King Abdullah University of Science and Technology, Thuwal, Saudi Arabia, as an Assistant Professor of electrical engineering. His current research interests include various aspects of computational electromagnetics with an emphasis on time-domain integral equations and their fast marching-on-in-time-based solutions, well-conditioned integral-equation formulations, and the development of fast hybrid methods for analyzing statistical EMC/EMI phenomena on complex and fully loaded platforms.

Dr. Bağcı was a recipient of the 2008 International Union of Radio Scientists Young Scientist Award and the 2004–2005 Interdisciplinary Graduate Fellowship from the Computational Science and Engineering Department, UIUC. His paper titled “Fast and Rigorous Analysis of EMC/EMI Phenomena on Electrically Large and Complex Structures Loaded with Coaxial Cables” was one of the three finalists (with honorable mention) for the 2008 Richard B. Schulz Best Transactions Paper Award given by the IEEE Electromagnetic Compatibility Society. He has authored or coauthored eight finalist papers in the student paper competitions at the 2005, 2008, and 2010 IEEE Antennas and Propagation Society International Symposiums and the 2013 and 2014 Applied Computational Electromagnetics Society Conferences.